A Novel Event-Triggered Load Frequency Control for Power Systems With Electric Vehicle Integration

Zhou Gu, *Senior Member, IEEE*, Yujian Fan, Tingting Yin, and Shen Yan

***Abstract*—This article proposes a novel even-triggered mechanism (ETM) to improve load frequency control (LFC) in power systems with electric vehicle (EV) integration, particularly when faced with bandwidth-constrained network communication. To mitigate the transmission of redundant packets that are typically found in conventional ETMs, a variable probabilistic release (VPR) scheme is introduced. The foundation of this VPR-based ETM rests on two crucial steps: 1) *Construction of an Event Generator With Variable Probability:* This generator facilitates the selection of actual released packets (ARPs) by using the VPR scheme from a group of triggered packets. Leveraging an algorithm, the probability of transmitting each triggered packet in the subsequent group is recomputed, enabling a more adaptive response to system dynamics. 2) *Setting a Buffer With Delay Effect:* A buffer is utilized to delay the release of ARPs until the final triggered instant in a group. The design not only simplifies timing division but also enhances system stability within fixed time intervals. Furthermore, this work formulates sufficient conditions that ensure the mean-square asymptotic stability (MSAS) of power systems. An illustrative example is presented to confirm the superiority of the proposed VPR-based ETM through comparative analysis with traditional ETMs.**

***Index Terms*—Load frequency control (LFC), power systems integration, variable gains, variable probabilistic release (VPR)-based even-triggered mechanism (ETM).**

I. Introduction

LOAD frequency control (LFC) is pivotal for ensuring frequency stability in traditional power systems, tasked with maintaining the system frequency at its nominal value and optimizing interarea tie-line power exchanges [1]. The frequency stability of power systems is a crucial indicator of power quality, directly impacting the reliable operation of the grid and user satisfaction [2], [3]. As power grids evolve with the integration of renewable energy sources and smart grid technologies, the role of LFC becomes even more crucial. The appearance of energy storage and distributed energy sources like solar and wind presents LFC with both challenges and opportunities. Energy storage systems store and release electricity, effectively balancing supply and demand and reducing frequency fluctuations. Modern LFC must thus account for the impact of diverse energy sources, including electric vehicles (EVs), to uphold system efficiency, reliability, and stability. EVs are increasingly recognized for their rapid response capabilities and distributed nature [4], providing an efficient and flexible solution for primary frequency regulation.

The integration of EVs and renewable energy sources into the power system has demonstrated numerous significant advantages. However, their random charging patterns significantly alter the load characteristics of the grid, complicating load forecasting and posing challenges to LFC systems. These challenges demand greater regulation capacity and faster response times from LFC. Consequently, optimizing LFC systems in the face of renewable energy integration, particularly EVs, has emerged as a critical research focus [5], [6], [7].

With the rapid development of large-scale interconnected power grids, traditional power system control methods relying on wired communication have shown limitations in scalability, cost-effectiveness, and flexibility. Consequently, the use of advanced communication networks for real-time and reliable signal transmission has become an attractive alternative. This approach meets the development needs of modern power grid intelligence and networking, providing strong technical support for the integration of EVs and renewable energy. This is the primary motivation behind the investigation presented in this article.

However, the integration of communication networks into power systems introduces a multitude of challenges in terms of system stability [8], [9], including communication delays [10], [11], constrained network bandwidth [3], [12], and malicious attacks [13], [14]. These issues are particularly pertinent in open transmission networks, leading to the increasing research interest in event-triggered LFC for power systems [15], [16], [17]. For instance, a dynamic periodic even-triggered mechanism (ETM) was developed for output feedback control systems to mitigate problems of limited network resources and external disturbances in [18]. In [19], event-triggered security adaptive control was designed for multiarea power systems, taking into account cyber attacks. Typically, the sampling period of an ETM remains constant to avoid the Zeno phenomenon [6]. The event generator employs predefined conditions to determine whether data should be

Received 22 July 2024; accepted 20 October 2024. Date of publication 30 October 2024; date of current version 18 December 2024. This work was supported in part by the National Natural Science Foundation of China under Grant 62273183 and Grant 62103193; in part by the Startup Funding of Anhui Polytechnic University under Grant 2024YQQ001; and in part by the Natural Science Foundation of Jiangsu Province of China under Grant BK20231288. This article was recommended by Associate Editor Y.-J. Kim. *(Corresponding author: Zhou Gu.)*

Zhou Gu is with the School of Electrical Engineering, Anhui Polytechnic University, Wuhu 241000, China, and also with the College of Mechanical and Electronic Engineering, Nanjing Forestry University, Nanjing 210037, China (e-mail: gzh1808@163.com).

Yujian Fan, Tingting Yin, and Shen Yan are with the College of Mechanical and Electronic Engineering, Nanjing Forestry University, Nanjing 210037, China.

Color versions of one or more figures in this article are available at https://doi.org/10.1109/TSMC.2024.3485164.

Digital Object Identifier 10.1109/TSMC.2024.3485164

transmitted to the controller via networks, significantly reducing data transmission and eases the burden on network resources. However, they still exhibit inherent limitations, such as relatively inflexible trigger condition designs and the generation of numerous unnecessary triggering data packets, when the system is approaching stability.

Recent years have witnessed various other trigger mechanisms, including memory-based [20], [21], integral-based [22], [23], dynamic memory-based [24], [25], segment-weighted information-based [26], and so on. These existing ETMs are categorized into two types: 1) static ETMs [27], [28] and 2) dynamic ETMs (DETMs) [29], [30]. Among these, DETMs have gained widespread approval due to their superior performance and broader application scope. For instance, Wang et al. [31] proposed a DETM using adaptive dynamic programming to implement LFC problems that consider denial-of-service (DoS) attacks. With the aid of an auxiliary dynamic variable, DETMs were developed to address LFC issues for continuous-time multiarea power systems in [24] and discrete-time multiarea power systems in [32]. In [33] and [34], the bounded and monotonic properties of the tanh function were applied to adjust the threshold of DETM, optimizing LFC performance and network bandwidth utilization. Both the auxiliary dynamic variable and the properties of the tanh function were used in [8] to further modify DETM for LFC issues. Despite this diversity, some issues remain to be addressed. For instance, unessential data packets are still triggered for potential transmission when the system approaches stability, reflecting a limitation inherent in these event-triggered conditions. Therefore, it is necessary and meaningful to develop a new mechanism to avoid this problem, which is another motivation for this article.

This article is dedicated to the development of a variable probabilistic release (VPR)-based ETM for LFC of power systems with EV integration. This innovative approach can not only further reduce the data-releasing rate (DRR) but also ensure the power system's control performance. The proposed VPR-based ETM begins with the creation of an event generator endowed with variable probability, responsible for selecting actual released packets (ARPs), and then a buffer is applied to delay the release of packets until the last triggering instant within the predefined triggered packet group. The stability of the power system with the VPR-based ETM can be ensured by variable feedback control gains that are obtained by the proposed algorithm. The main contributions of this article can be summarized as follows.

1) A novel VPR-based ETM is first proposed to reduce the number of transmitted packets, thereby further reducing the DRR. This approach addresses a key limitation of traditional event-triggered mechanisms (TETMs), such as those in [27], where a large number of sampling instants are triggered even when the system is stable, resulting in unnecessary data transmission.
2) Within the TETM framework, a VPR strategy is introduced, and an algorithm is developed to obtain variable feedback control gains for LFC power systems. Unlike existing event-based control methods, such as those in [35], our approach dynamically updates the release probability in subsequent groups and adjusts the control gains, resulting in improved control performance for LFC power systems.

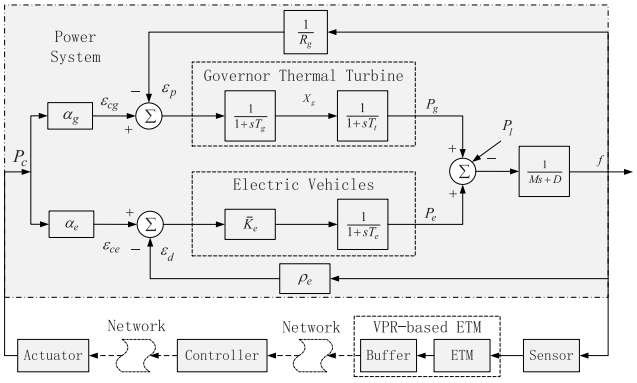

Fig. 1. Structure of VPR ETM-based power system with EVs.

The remainder of this article is organized as follows. The system description and the model of the VPR-based ETM are presented in Section II. Section III offers the main results of the proposed method that used in LFC power systems with EVs integration. A practical example using the proposed VPR-based ETM is provided in Section IV to manifest the validity of theoretical results. Section V concludes this article.

Notation: In this article, some symbols are defined as follows: $\lceil x \circ P \rceil = x^T P x$; $\mathcal{G}^l = \{1, 2, \ldots, l\}$, l is a given constant; $\mathbb{C}\{X, Y\} = [X^T \ Y^T]^T$; $\mathbb{D}\{X, Y\} = \text{diag}\{X \ Y\}$ denotes a diagonal matrix; $\mathbb{C}_{m=1}^{l}\{X_m\} = [X_1^T \ X_2^T \ \cdots \ X_l^T]^T$; $\mathbb{D}_{m=1}^{l}\{Y_m\} = \text{diag}\{Y_1 \ Y_2 \ \cdots \ Y_l\}$; $\mathbb{C}_1^l\{Y\} = [\underbrace{Y^T \ Y^T \ \cdots \ Y^T}_{l}]^T$; $\mathbb{D}_1^l\{Y\} = \text{diag}\{\underbrace{Y \ Y \ \cdots \ Y}_{l}\}$.

II. Problem Formulation

A. System Description

According to [8] and Fig. 1, the primary frequency signals from the thermal power plant and EVs are described as follows:

$$\varepsilon_p(t) = \frac{1}{R_g} f(t), \ \ \varepsilon_d(t) = \rho_e f(t) \tag{1}$$

where $f(t)$ is the frequency deviation; R_g and ρ_e denote the droop characteristic of governor and EVs, respectively. $P_c(t)$ in Fig. 1, represents the control input; and α_g and α_e denote participation factors originating from the secondary frequency control signals of the thermal power plant and EVs. Then, the control signals can be represented by

$$\varepsilon_{cg}(t) = \alpha_g P_c(t), \ \ \varepsilon_{ce}(t) = \alpha_e P_c(t). \tag{2}$$

The LFC signals to thermal plant and EVs can be formulated as follows:

$$\varepsilon_g(t) = \varepsilon_{cg}(t) - \varepsilon_p(t), \ \ \varepsilon_e(t) = \varepsilon_{ce}(t) - \varepsilon_d(t). \tag{3}$$

According to [36], we know that the deviations of governor value position and turbine output power are

$$\dot{X}_g(t) = -\frac{1}{T_g R_g} f(t) - \frac{1}{T_g} X_g(t) + \frac{\alpha_g}{T_g} P_c(t)$$
$$\dot{P}_g(t) = \frac{1}{T_t} X_g(t) - \frac{1}{T_t} P_g(t). \tag{4}$$

Also, the dynamics of EVs can be expressed by [8]

$$\dot{P}_e(t) = -\frac{\rho_e \bar{K}_e}{T_e} f(t) - \frac{1}{T_e} P_e(t) + \frac{\alpha_e \bar{K}_e}{T_e} P_c(t) \tag{5}$$

where T_e is a time constant and $\bar{K}_e$ is a control gain of EVs.

The dynamic of the system frequency is given by

$$\dot{f}(t) = -\frac{D}{M} f(t) + \frac{1}{M}\big(P_g(t) + P_e(t) - P_l(t)\big) \tag{6}$$

where D and M are the load damping coefficient and inertia constant in the power systems, respectively. $P_l(t)$ represents the external disturbance.

Define $x^T(t) \triangleq [f(t)\ X_g(t)\ P_g(t)\ P_e(t)\ \Delta(t)] \in \mathbb{R}^5$ and $y^T(t) \triangleq [f(t)\ \Delta(t)] \in \mathbb{R}^2$ as state variables and performance outputs, and $u(t) \triangleq P_c(t) \in \mathbb{R}$ as the control input of LFC. The area error control $bf(t)$ is adopted to maintain the zero steady-state error for frequency deviation, where b is the frequency bias constant, and its integral form, denoted as $\Delta(t) = \int bf(t)dt$, is an auxiliary variable designed to improve steady-state performance.

Combining (1)–(6) follows that:

$$\begin{cases} \dot{x}(t) = Ax(t) + B_u u(t) + B_w \omega(t) \\ y(t) = Cx(t) \end{cases} \tag{7}$$

where $\omega(t) \triangleq P_l(t) \in \mathbb{R}$ denotes the external disturbance; and A, B_u, B_w, and C are the system matrices with

$$A = \begin{bmatrix} -\frac{D}{M} & 0 & \frac{1}{M} & \frac{1}{M} & 0 \\ -\frac{1}{R_g T_g} & -\frac{1}{T_g} & 0 & 0 & 0 \\ 0 & \frac{1}{T_t} & -\frac{1}{T_t} & 0 & 0 \\ -\frac{\rho_e \bar{K}_e}{T_e} & 0 & 0 & -\frac{1}{T_e} & 0 \\ b & 0 & 0 & 0 & 0 \end{bmatrix}, B_u = \begin{bmatrix} 0 \\ \frac{\alpha_g}{T_g} \\ 0 \\ \frac{\alpha_e \bar{K}_e}{T_e} \\ 0 \end{bmatrix}$$
$$B_w^T = \begin{bmatrix} -\frac{1}{M} & 0 & 0 & 0 & 0 \end{bmatrix}, C = \begin{bmatrix} 1 & 0 & 0 & 0 & 0 \\ 0 & 0 & 0 & 0 & 1 \end{bmatrix}.$$

B. Design of the VPR-Based ETM

First, we introduce the TETM [37]

$$t_{k+1}h = t_k h + \min_{j \in N} \{jh | \Psi(e(t), x(t_k h), \delta) > 0\} \tag{8}$$

where $e(t) = x(t_k h + jh) - x(t_k h)$, $t \in [t_k h + jh, t_k h + jh + h)$ and $x(t_k h + jh)$ are the state vector error and current sampling state value, respectively; δ is a given constant; and $\Psi(e(t), x(t_k h), \delta) = \lceil e(t) \circ \Theta \rceil - \delta(\lceil x(t_k h) \circ \Theta \rceil)$, and Θ is a weight matrix to be designed.

Obviously, the usage of the ETM (8) consumes less network bandwidth in contrast to periodic sampling transmission methods. However, relying solely on the ETM (8) results in the transmission of a considerable amount of unnecessary data over the network, especially when the system approaches stability. To tackle this issue, we develop a VPR scheme: a predefined number of sequential packets that meet the triggering condition in (8) are stored in the buffer. One of these packets is selected as the ARP and is released at the final triggered instant within this group. For example, l triggered packets in the nth group is given as

$$x(t_{k+1}h)|_{\beta_1^n};\ x(t_{k+2}h)|_{\beta_2^n}; \cdots\ x(t_{k+l}h)|_{\beta_l^n}$$

where $x(t_{k+m}h)$ with $m = 1, 2, \ldots, l$ is the system state at triggering instant; and β_l^n is an independent random variable following the $0-1$ distribution: $\beta_l^n \sim B(1, \bar{\beta}_l^n)$ with the constraint $\sum_{m=1}^{l} \beta_m^n = 1$. Here, $\beta_m^n = 1$ indicates that the data at corresponding instant should be released, while the rest packets within the nth group are discarded.

Here, we define the packet at $z_n h$ is an ARP governed by the $0-1$ distribution, where $n \in N_+$ and $z_n h \in \mathbb{T}_l = \{t_{k+1}h, t_{k+2}h, , \ldots, t_{k+l}h\}$ with $k = (n-1)(l-1)$.

To gain a deeper understanding of the principles underlying the proposed VPR-based ETM, we take $l = 3$ as an example to interpret possible transmission scenarios. Suppose the time-sequence is as depicted in Fig. 2. Four groups are presented: $\{t_1 h, t_2 h, t_3 h\}$, $\{t_3 h, t_4 h, t_5 h\}$, $\{t_5 h, t_6 h, t_7 h\}$, $\{t_7 h, t_8 h, t_9 h\}$. Followed by the $0-1$ distribution with the probability distribution parameter, $t_1 h(z_1 h)$ in the first group, $t_4 h(z_2 h)$ in the second group, $t_7 h(z_3 h)$ in the third group and $t_8 h(z_4 h)$ in the fourth group, and so on, are selected as the ARPs at those instants. It should be mentioned that these ARPs are not released at their corresponding instants but at the instant of the last packet in their respective groups, by which it simplifies the stability analysis. These actual released instants (ARIs) are $t_3 h, t_5 h, t_7 h$ and $t_9 h, \ldots$. In addition, d_n is the waiting time of the ARP for release in the nth group.

According to the properties of $0-1$ distribution, we have: $E\{\beta_m^n = 1\} = \bar{\beta}_m^n$, $E\{\beta_m^n - \bar{\beta}_m^n\} = 0$ and $E\{(\beta_m^n - \bar{\beta}_m^n)^2\} = (\hat{\beta}_m^n)^2$. In order to achieve a reasonable data selection, we define the selection probability of each trigged packet as follows:

$$\bar{\beta}_m^{n+1} = \frac{\|x(t_{k+m}h) - x(z_n h)\|}{\sum_{m=1}^{l} \|x(t_{k+m}h) - x(z_n h)\|} \tag{9}$$

where $x(z_n h)$ is the ARP in the nth group; and $x(t_{k+m}h)$ and $\bar{\beta}_m^{n+1}$, $m \in \mathcal{G}^l$ are the mth triggered packet in the $(n+1)$th group and the expectation of its transmission probability, respectively. For a clearer description, we still take Fig. 2 as an example. The probabilities of selecting each triggered packet in the third group can be calculated as follows: $\bar{\beta}_1^3 = \|x(t_5 h) - x(z_2 h)\| / \sum_{m=1}^{3} \|x(t_{4+m}h) - x(z_2 h)\|$, $\bar{\beta}_2^3 = \|x(t_6 h) - x(z_2 h)\| / \sum_{m=1}^{3} \|x(t_{4+m}h) - x(z_2 h)\|$ and $\bar{\beta}_3^3 = \|x(t_7 h) - x(z_2 h)\| / \sum_{m=1}^{3} \|x(t_{4+m}h) - x(z_2 h)\|$.

Based on the above discussion, we can develop the following VPR-based ETM as:

$$t_{k+m+1}h = t_{k+m}h + \min_{p \in \mathbb{Z}_{\geq 0}} \left\{ ph | \tilde{\Psi}\big(e_m^n(t), x(t_{k+m}h), \delta\big) > 0 \right\} \tag{10}$$

where $m \in \mathcal{G}^{l-1}$, and $\tilde{\Psi}(e_m^n(t), x(t_{k+m}h), \delta) = \lceil e_m^n(t) \circ \Theta \rceil - \delta(\lceil x(t_{k+m}h) \circ \Theta \rceil)$ and $e_m^n(t) = x(t_{k+m}h) - x(t_{k+m}h + ph)$ is the m-th state error in the n-th group.

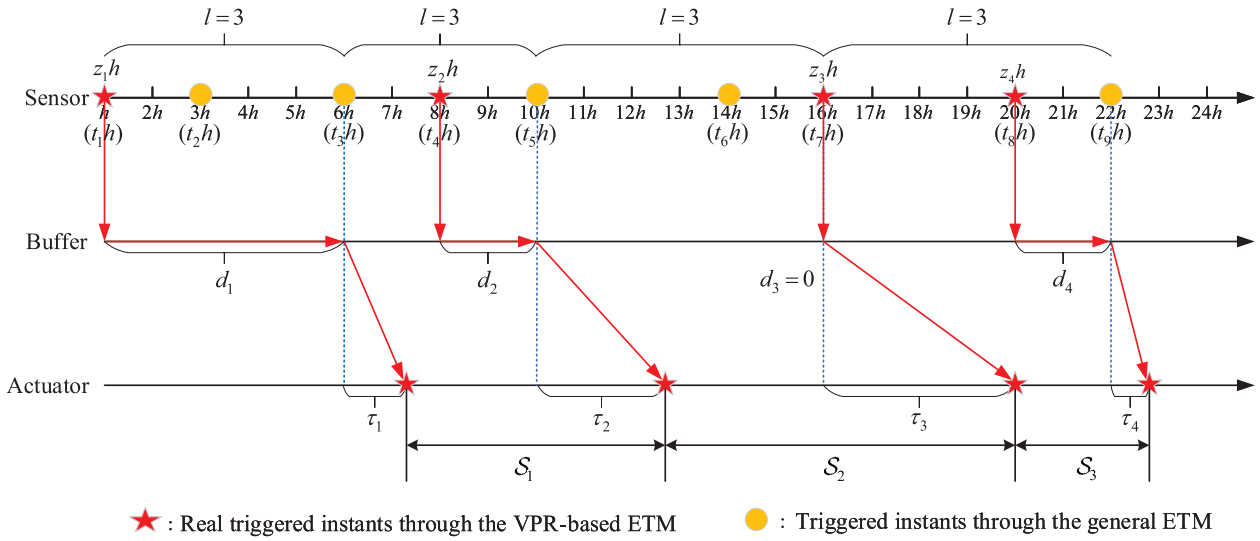

Fig. 2. Example of time-sequence for ($l = 3$).

Inspired by [38], we define

$$\eta_m^n(t) = t - t_{k+m}h - ph \tag{11}$$

where $m \in \mathcal{G}^l$ and $t \in [t_{k+m}h + \eta_{k+m},\ t_{k+m+1}h + \eta_{k+m+1})$.

Then, we have

$$e_m^n(t) = x(t_{k+m}h) - x\big(t - \eta_m^n(t)\big). \tag{12}$$

Remark 1: The proposed VPR-based ETM will be reduced to the TETM, if one sets $l = 1$ in (10). According to the constraint $\sum_{m=1}^{l} \beta_m^n = 1$ with $l = 1$, one has $\beta_1^n = 1$. This means there are no other triggered packets to choose as an ARP in the nth group, and the mechanism becomes the TETM.

Remark 2: In Fig. 2, $z_3h(t_7h)$ is the last triggered packet within the third group, serving as the ARI in the this group. For this scenario, $d_3 = 0$. As $\|x(t_7h) - x(z_3h)\| = 0$, we deduce that $\bar{\beta}_1^4 = 0$. Consequently, we can conclude that in this scenario the packet at ARI can not coincide with the ARP in the subsequent group due to the probability constrain defined in (9).

Define $\mathcal{S}_n = [z_nh + d_n + \tau_n,\ z_{n+1}h + d_{n+1} + \tau_{n+1})$, where τ_n is the transmission delay of the ARP in the nth group, and $d_n = t_{n(l-1)+1}h - z_nh$. Assume $\max\{\tau_n + d_n\} = \bar{\tau}_d$ and $\bar{\tau}_d + h = \tau_M$.

Then, similar to (11) and (12), we define

$$\tau_m^n(t) = t - t_{k+m}h - ph \tag{13}$$

$$e_m^n(t) = x(t_{k+m}h) - x\big(t - \tau_m^n(t)\big) \tag{14}$$

for $t \in \mathcal{S}_n$, where $m \in \mathcal{G}^l$ and $n \in N_+$. From (13), it is known that $\tau_m^n(t)$ contains the information of the waiting delay d_n and the transmission delay τ_n.

Under the above VPR-based ETM, we can express the state variable at z_nh for $t \in \mathcal{S}_n$ as

$$\begin{aligned} x(z_nh) &= \sum_{m=1}^{l-1} \beta_m^n x(t_{k+m}h) + \left(1 - \sum_{m=1}^{l-1} \beta_m^n\right) x(t_{k+l}h) \\ &= \sum_{m=1}^{l-1} \beta_m^n \Phi_m^n(t) + \left(1 - \sum_{m=1}^{l-1} \beta_m^n\right) \Phi_l^n(t) \end{aligned} \tag{15}$$

where $\Phi_m^n(t) = e_m^n(t) + x(t - \tau_m^n(t))$.

In this study, we assume the states in (7) are measurable. Based on this assumption, we design the following state feedback controller using the aforementioned VPR-based ETM:

$$\begin{aligned} u(t) &= K_n x(z_nh) \\ &= \sum_{m=1}^{l-1} \beta_m^n K_n \Phi_m^n(t) + \left(1 - \sum_{m=1}^{l-1} \beta_m^n\right) K_n \Phi_l^n(t) \end{aligned} \tag{16}$$

for $t \in \mathcal{S}_n$, where K_n represents the controller gain to be designed, utilizing the data packet from the nth group.

Remark 3: Following the VPR scheme, the controller gain is updated when the selection probability in (9) exceeds a defined threshold. An algorithm will be presented in the subsequent sections to implement the proposed control strategy.

C. Closed-Loop System With the VPR-Based ETM

Based on (16), one can get the closed-loop power system with VPR-based ETM as

$$\begin{cases} \dot{x}(t) = \phi(t) + \varphi(t) \\ y(t) = Cx(t) \end{cases} \tag{17}$$

for $t \in \mathcal{S}_n$, where

$$\begin{aligned} \phi(t) &= Ax(t) + \sum_{m=1}^{l-1} \bar{\beta}_m^n B_u K_n \Phi_m^n(t) \\ &\quad + \left(1 - \sum_{m=1}^{l-1} \bar{\beta}_m^n\right) B_u K_n \Phi_l^n(t) + B_w \omega(t) \\ \varphi(t) &= \sum_{m=1}^{l-1} (\beta_m^n - \bar{\beta}_m^n) B_u K_n \Phi_m^n(t) \\ &\quad + \sum_{m=1}^{l-1} (\bar{\beta}_m^n - \beta_m^n) B_u K_n \Phi_l^n(t). \end{aligned}$$

In this study, our objective is to develop a control strategy and a VPR-based ETM with the goals of achieving mean-square asymptotic stability (MSAS) for the LFC power system in (17) under the absence of external disturbances (i.e., $P_l(t) = 0$) and

ensuring H_∞ stability of the LFC power system in the presence of external disturbances $P_l(t)$ when $P_l(t) \neq 0$.

III. Main Results

Before analyzing the MSAS of closed-loop system (17), we give the following denotations:

$$\begin{aligned}
\zeta^T(t) &= \left[x^T(t)\ \zeta_1^T(t)\ x^T(t-\tau_M)\ \zeta_2^T(t)\ \omega^T(t)\right] \\
\zeta_1(t) &= \mathbb{C}_{m=1}^{l}\{x\big(t-\tau_m^n(t)\big)\}, \quad \zeta_2(t) = \mathbb{C}_{m=1}^{l}\{e_m^n(t)\} \\
\mathscr{I}_s &= \left[0_{5\times 5(s-1)}\ I_{5\times 5}\ 0_{5\times 5(2l+2-s)}\ 0_{5\times 1}\right],\ s \in \mathcal{G}^{2l+2} \\
\mathscr{I}_\omega &= \left[0_{5\times 5(2l+2)}\ 1_{5\times 1}\right], \mathbf{1}^T = [1\ 1\ 1\ 1\ 1] \\
\mathcal{Z}_v &= \left[0_{5\times 5(v-1)}\ I_{5\times 5}\ 0_{5\times 5(3-v)}\right], v = 1,\quad 2,\quad 3
\end{aligned}$$

for $t \in \mathcal{S}_n$.

Theorem 1: Under the proposed VPR-based ETM in (10), the LFC power system in (17) with the control strategy in (16) is MSAS with H_∞ norm bound γ, if there exist symmetric matrices $P > 0$, $Q > 0$, $R_m > 0$, $\Theta > 0$ and matrices S_m, such that

$$\Pi_n < 0 \tag{18}$$

$$\begin{bmatrix} R_m & * \\ S_m & R_m \end{bmatrix} \geq 0 \tag{19}$$

hold for $m \in \mathcal{G}^l$, where δ, $\bar{\beta}_i^n$, $\hat{\beta}_i^n$, $i \in \mathcal{G}^{l-1}$, $n \in N_+$, l are given scalars, K_n is a prescribed matrix, and

$$\begin{aligned}
\Pi_n &= \mathbf{He}\big(\mathcal{A}^T P \mathscr{I}_1\big) + \lceil \mathscr{I}_1 \circ Q \rceil + \lceil \mathscr{I}_{l+2} \circ Q \rceil \\
&\quad + \sum_{m=1}^{l}\Bigg(\lceil(\tau_M \mathcal{A}) \circ R_m\rceil + \sum_{i=1}^{l-1}\Big(\Big\lceil\Big(\tau_M \hat{\beta}_i^n \mathcal{B}_i\Big) \circ R_m\Big\rceil\Big) \\
&\quad + \lceil \mathcal{C}_m \circ \Gamma_m\rceil + \delta\big(\lceil(\mathscr{I}_{l+2+m} + \mathscr{I}_{m+1}) \circ \Theta\rceil\big) \\
&\quad - \lceil \mathscr{I}_{l+2+m} \circ \Theta\rceil\Bigg) + \lceil (C\mathscr{I}_1) \circ I_c\rceil \\
&\quad - \gamma^2\Big(\Big\lceil\Big(\frac{1}{5}\mathbf{1}^T\mathbf{1}\mathscr{I}_\omega\Big) \circ I_\omega\Big\rceil\Big) \\
\mathcal{A} &= A\mathscr{I}_1 + \sum_{i=1}^{l-1}\bar{\beta}_i^n B_u K_n(\mathscr{I}_{i+1} + \mathscr{I}_{l+2+i}) \\
&\quad + \Big(1 - \sum_{i=1}^{l-1}\bar{\beta}_i^n\Big)B_u K_n(\mathscr{I}_{l+1} + \mathscr{I}_{2l+2}) + \frac{1}{5}B_\omega \mathbf{1}^T\mathbf{1}\mathscr{I}_\omega \\
\mathcal{B}_i &= B_u K_n(\mathscr{I}_{l+2+i} - \mathscr{I}_{2l+2} + \mathscr{I}_{i+1} - \mathscr{I}_{l+1}) \\
\mathcal{C}_m &= \left[\mathscr{I}_1^T\ \mathscr{I}_{m+1}^T\ \mathscr{I}_{l+2}^T\right]^T \\
\Gamma_m &= -\lceil \mathcal{Z}_1 \circ R_m\rceil + \mathbf{He}\{\mathcal{Z}_2^T(R_m - S_m)\mathcal{Z}_1\} \\
&\quad + \mathbf{He}\{\mathcal{Z}_3^T S_m \mathcal{Z}_1\} + \left\lceil \mathcal{Z}_2 \circ \big(S_m^T + S_m - 2R_m\big)\right\rceil \\
&\quad + \mathbf{He}\{\mathcal{Z}_3^T(R_m - S_m)\mathcal{Z}_2\} - \lceil \mathcal{Z}_3 \circ R_m\rceil.
\end{aligned}$$

Proof: Construct the following Lyapunov functional:

$$V(t) = \lceil x(t) \circ P\rceil + \sum_{i=1}^{2} V_i(t) \tag{20}$$

where $V_1(t) = \int_{t-\tau_M}^{t}\lceil x(s) \circ Q\rceil ds$ and $V_2(t) = \tau_M \sum_{m=1}^{l}\int_{-\tau_M}^{0}\int_{t+\theta}^{t}\lceil \dot{x}(s) \circ R_m\rceil ds d\theta$.

Note that

$$E\big\{\mathbf{He}\big(\dot{x}^T(t)Px(t)\big)\big\} = E\Big\{\lceil \zeta(t) \circ \mathbf{He}\big(\mathcal{A}^T P \mathscr{I}_1\big)\rceil\Big\} \tag{21}$$

where

$$\begin{aligned}
\mathcal{A} &= A\mathscr{I}_1 + \sum_{i=1}^{l-1}\bar{\beta}_i^n B_u K_n(\mathscr{I}_{i+1} + \mathscr{I}_{l+2+i}) \\
&\quad + \Big(1 - \sum_{i=1}^{l-1}\bar{\beta}_i^n\Big)B_u K_n(\mathscr{I}_{l+1} + \mathscr{I}_{2l+2}) + \frac{1}{5}B_\omega \mathbf{1}^T\mathbf{1}\mathscr{I}_\omega.
\end{aligned}$$

Taking the derivative with respect to V_1 leads to

$$E\{\dot{V}_1(t)\} = E\big\{\lceil \zeta(t) \circ (\lceil \mathscr{I}_1 \circ Q\rceil + \lceil \mathscr{I}_{l+2} \circ Q\rceil)\rceil\big\}. \tag{22}$$

Applying Jensen inequality, (19), we have

$$\begin{aligned}
E\{\dot{V}_2(t)\} \leq \sum_{m=1}^{l} E\Bigg\{\Bigg\lceil \zeta(t) \circ \Bigg\{\lceil(\tau_M \mathcal{A}) \circ R_m\rceil \\
+ \sum_{i=1}^{l-1}\Big(\Big\lceil\Big(\tau_M \hat{\beta}_i^n \mathcal{B}_i\Big) \circ R_m\Big\rceil\Big) + \lceil \mathcal{C}_m \circ \Gamma_m\rceil\Bigg\}\Bigg\rceil\Bigg\}.
\end{aligned} \tag{23}$$

From (10), it yields that

$$\begin{aligned}
\sum_{m=1}^{l}\Bigg\{\Bigg\lceil \zeta(t) \circ \Big(\delta\big(\lceil(\mathscr{I}_{l+2+m} + \mathscr{I}_{m+1}) \circ \Theta\rceil\big) \\
- \lceil \mathscr{I}_{l+2+m} \circ \Theta\rceil\Big)\Bigg\rceil\Bigg\} > 0.
\end{aligned} \tag{24}$$

Define the following H_∞ performance index:

$$\begin{aligned}
\mathcal{J}(t) &= \|y(t)\|_2^2 - \gamma^2\|\omega(t)\|_2^2 \\
&= \lceil \zeta(t) \circ (\lceil (C\mathscr{I}_1) \circ I_c\rceil)\rceil \\
&\quad - \gamma^2\Big\lceil \zeta(t) \circ \Big(\lceil\Big(\frac{1}{5}\mathbf{1}^T\mathbf{1}\mathscr{I}_\omega\Big) \circ I_\omega\rceil\Big)\Big\rceil
\end{aligned} \tag{25}$$

where I_c and I_ω are identity matrices with appropriate dimensions, and γ is a given constant.

Combining (20)–(25), we have

$$\begin{aligned}
&E\{\dot{V}(t)\} + \mathcal{J}(t) - \mathcal{J}(t) \\
&\leq E\Bigg\{\lceil \zeta(t) \circ \Big[\mathbf{He}\big(\mathcal{A}^T P \mathscr{I}_1\big) + \lceil \mathscr{I}_1 \circ Q\rceil + \lceil \mathscr{I}_{l+2} \circ Q\rceil \\
&\quad + \sum_{m=1}^{l}\Bigg(\lceil(\tau_M \mathcal{A}) \circ R_m\rceil + \sum_{i=1}^{l-1}\Big(\Big\lceil\Big(\tau_M \hat{\beta}_i^n \mathcal{B}_i\Big) \circ R_m\Big\rceil\Big) \\
&\quad + \lceil \mathcal{C}_m \circ \Gamma_m\rceil + \delta\big(\lceil(\mathscr{I}_{l+2+m} + \mathscr{I}_{m+1}) \circ \Theta\rceil\big) \\
&\quad - \lceil \mathscr{I}_{l+2+m} \circ \Theta\rceil\Bigg)\Bigg\rceil\Bigg\} + \lceil \zeta(t) \circ (\lceil (C\mathscr{I}_1) \circ I_c\rceil)\rceil \\
&\quad - \lceil \zeta(t) \circ (\lceil (C\mathscr{I}_1) \circ I_c\rceil)\rceil \\
&\quad - \gamma^2\Big\lceil \zeta(t) \circ \Big(\Big\lceil\Big(\frac{1}{5}\mathbf{1}^T\mathbf{1}\mathscr{I}_\omega\Big) \circ I_\omega\Big\rceil\Big)\Big\rceil \\
&\quad + \gamma^2\Big\lceil \zeta(t) \circ \Big(\Big\lceil\Big(\frac{1}{5}\mathbf{1}^T\mathbf{1}\mathscr{I}_\omega\Big) \circ I_\omega\Big\rceil\Big)\Big\rceil \\
&= E\{\lceil \zeta(t) \circ \Pi_n\rceil\} - \mathcal{J}(t).
\end{aligned}$$

Then, one can conclude from (18) that

$$E\{\dot{V}(t)\} \leq -\mathcal{J}(t). \tag{26}$$

Integrating (26) from t_0 to ∞ leads to

$$V(\infty) - V(t_0) \leq \int_{t_0}^{\infty}\Big[-y^T(t)y(t) + \gamma^2\omega^T(t)\omega(t)\Big]dt \tag{27}$$

for all $0 \neq \omega(t) \in L_2[t_0,\ \infty)$.

Under zero initial condition, one has

$$\int_{t_0}^{\infty} y^T(t)y(t)dt \le \int_{t_0}^{\infty} \gamma^2\omega^T(t)\omega(t)dt.$$

In addition, from (25) and (26) one knows that the LFC power system (17) is MSAS. The proof is completed. ■

In Theorem 1, K_n is a given matrix. Next, we will design the controller gains and the weight matrix of the VPR-based ETM based on Theorem 1.

Theorem 2: Under the proposed VPR-based ETM in (10), the LFC power system in (17) with the control strategy in (16) is MSAS with H_∞ norm bound γ, if there exist symmetric matrices $X_n > 0$, $\tilde{Q} > 0$, $\tilde{R}_m > 0$, $\tilde{\Theta} > 0$ and matrices $\tilde{S}_m$, such that

$$\begin{bmatrix} \tilde{\Pi}_1^n & * \\ \tilde{\Pi}_2^n & \tilde{\Pi}_3^n \end{bmatrix} < 0 \tag{28}$$

$$\begin{bmatrix} \tilde{R}_m & * \\ \tilde{S}_m & \tilde{R}_m \end{bmatrix} \ge 0 \tag{29}$$

hold for $m \in \mathcal{G}^l$, where ρ, δ, $\bar{\beta}_i^n$, $\hat{\beta}_i^n$, $i \in \mathcal{G}^{l-1}$, $n \in N_+$, l are given scalars, and

$$\begin{aligned}
\tilde{\Pi}_1^n &= \mathbf{He}\left(\tilde{\mathcal{A}}^T\mathscr{I}_1\right) + \lceil\mathscr{I}_1 \circ \tilde{Q}\rceil + \lceil\mathscr{I}_{l+2} \circ \tilde{Q}\rceil \\
&\quad + \sum_{m=1}^{l}\Big(\lceil\mathcal{C}_m \circ \tilde{\Gamma}_m\rceil + \delta\big(\lceil(\mathscr{I}_{l+2+m} + \mathscr{I}_{m+1}) \circ \tilde{\Theta}\rceil\big) \\
&\quad - \lceil\mathscr{I}_{l+2+m} \circ \tilde{\Theta}\rceil\Big) - \gamma^2\Big(\lceil\Big(\frac{1}{5}\mathbf{1}^T\mathbf{1}\mathscr{I}_\omega\Big) \circ I_\omega\rceil\Big) \\
\tilde{\Pi}_2^n &= \mathbb{C}\{\tilde{\Pi}_2^1,\ \tilde{\Pi}_2^2,\ CX_n\mathscr{I}_1\} \\
\tilde{\Pi}_3^n &= \mathbb{D}\{\tilde{\Pi}_3^1,\ \tilde{\Pi}_3^2,\ -I\} \\
\tilde{\Pi}_2^1 &= \mathbb{C}_1^l\{\tau_M\tilde{\mathcal{A}}\},\ \tilde{\Pi}_2^2 = \mathbb{C}_1^l\big\{\mathbb{C}_{i=1}^{l-1}\{\tau_M\hat{\beta}_i^n\tilde{\mathcal{B}}_i\}\big\} \\
\tilde{\Pi}_3^1 &= \mathbb{D}_{m=1}^l\{\rho^2\tilde{R}_m - 2\rho X_n\} \\
\tilde{\Pi}_3^2 &= \mathbb{D}_{m=1}^l\big\{\mathbb{D}_1^{l-1}\{\rho^2\tilde{R}_m - 2\rho X_n\}\big\} \\
\tilde{\mathcal{A}} &= AX_n\mathscr{I}_1 + \sum_{i=1}^{l-1}\bar{\beta}_i^n B_u Y_n(\mathscr{I}_{i+1} + \mathscr{I}_{l+2+i}) \\
&\quad + \left(1 - \sum_{i=1}^{l-1}\bar{\beta}_i^n\right)B_u Y_n(\mathscr{I}_{l+1} + \mathscr{I}_{2l+2}) + \frac{1}{5}B_\omega\mathbf{1}^T\mathbf{1}\mathscr{I}_\omega \\
\tilde{\mathcal{B}}_i &= B_u Y_n(\mathscr{I}_{l+2+i} - \mathscr{I}_{2l+2} + \mathscr{I}_{i+1} - \mathscr{I}_{l+1}) \\
\tilde{\Gamma}_m &= -\lceil\mathcal{Z}_1 \circ \tilde{R}_m\rceil + \mathbf{He}\{\mathcal{Z}_2^T\left(\tilde{R}_m - \tilde{S}_m\right)\mathcal{Z}_1\} \\
&\quad + \mathbf{He}\{\mathcal{Z}_3^T\tilde{S}_m\mathcal{Z}_1\} + \left\lceil\mathcal{Z}_2 \circ \left(\tilde{S}_m^T + \tilde{S}_m - 2\tilde{R}_m\right)\right\rceil \\
&\quad + \mathbf{He}\{\mathcal{Z}_3^T\left(\tilde{R}_m - \tilde{S}_m\right)\mathcal{Z}_2\} - \lceil\mathcal{Z}_3 \circ \tilde{R}_m\rceil.
\end{aligned}$$

Furthermore, the controller gains and the weight matrix of the proposed VPR-based ETM are: $K_n = Y_nX_n^{-1}$ and $\Theta_n = \lceil X_n^{-1} \circ \tilde{\Theta}\rceil$, respectively.

Proof: Define $X_n = P^{-1}$, $\tilde{Q} = \lceil X_n \circ Q\rceil$, $\tilde{R}_m = \lceil X_n \circ R_m\rceil$, $\tilde{S}_m = \lceil X_n \circ S_m\rceil$, $\Im = \text{diag}\{\mathcal{Q}\ I\}$ with $\mathcal{Q} = \mathbb{D}_{s=1}^3\{\mathcal{Q}_s\}$, where $\mathcal{Q}_1 = \text{diag}\{\mathbb{D}_1^{2l+2}\{X_n\}\ I\}$, $\mathcal{Q}_2 = \mathbb{D}_{m=1}^l\{R_m^{-1}\}$ and $\mathcal{Q}_3 = \mathbb{D}_{m=1}^l\{\mathbb{D}_1^{l-1}\{R_m^{-1}\}\}$.

Algorithm 1 Acquisition of K_{n+1}, Θ_{n+1}, and $\bar{\beta}_m^{n+1}$

Input: Parameters required in Theorem 2;
Output: K_{n+1}, Θ_{n+1} and $\bar{\beta}_m^{n+1}$;
1: Initialize the parameters $\bar{\beta}_m^1$, $\forall m \in \mathcal{G}^l$, and $n = 1$;
2: Solve K_1, Θ_1 in terms of Theorem 2;
3: Calculate $\bar{\beta}_m^{n+1}$ according (9);
4: **if** $\|\bar{\beta}_m^{n+1} - \bar{\beta}_m^n\| < \varepsilon$ for all $m \in \mathcal{G}^l$ **then**
5: $K_{n+1} = K_n$, $\Theta_{n+1} = \Theta_n$;
6: **else**
7: Solve K_{n+1}, Θ_{n+1} from Theorem 2 by using LMI toolbox;
8: **if** no solution in Step 7 **then**
9: $K_{n+1} = K_n$, $\Theta_{n+1} = \Theta_n$, $\bar{\beta}_m^{n+1} = \bar{\beta}_m^n$;
10: **else**
11: Output K_{n+1}, Θ_{n+1} and $\bar{\beta}_m^{n+1}$;
12: **end if**
13: **end if**
14: n=n+1;
15: Go to Step 3;

By applying Schur complement, (18) can be rewritten as

$$\begin{bmatrix} \Pi_1^n & * \\ \Pi_2^n & \Pi_3^n \end{bmatrix} < 0 \tag{30}$$

where

$$\begin{aligned}
\Pi_1^n &= \mathbf{He}\big(\mathcal{A}^TP\mathscr{I}_1\big) + \lceil\mathscr{I}_1 \circ Q\rceil + \lceil\mathscr{I}_{l+2} \circ Q\rceil \\
&\quad + \sum_{m=1}^{l}\Big(\lceil\mathcal{C}_m \circ \Gamma_m\rceil + \delta\big(\lceil(\mathscr{I}_{l+2+m} + \mathscr{I}_{m+1}) \circ \Theta\rceil\big) \\
&\quad - \lceil\mathscr{I}_{l+2+m} \circ \Theta\rceil\Big) - \gamma^2\left\lceil\left(\frac{1}{5}\mathbf{1}^T\mathbf{1}\mathscr{I}_\omega\right) \circ I_\omega\right\rceil \\
\Pi_2^n &= \mathbb{C}\{\Pi_2^1,\ \Pi_2^2,\ C\mathscr{I}_1\} \\
\Pi_3^n &= \mathbb{D}\{\Pi_3^1,\ \Pi_3^2,\ -I\} \\
\Pi_2^1 &= \mathbb{C}_{m=1}^l\{R_m\tau_M\mathcal{A}\},\ \Pi_2^2 = \mathbb{C}_{m=1}^l\big\{\mathbb{C}_{i=1}^{l-1}\{\tau_M\hat{\beta}_i^nR_m\mathcal{B}_i\}\big\} \\
\Pi_3^1 &= \mathbb{D}_{m=1}^l\{-R_m\},\ \Pi_3^2 = \mathbb{D}_{m=1}^l\big\{\mathbb{D}_1^{l-1}\{-R_m\}\big\}.
\end{aligned}$$

Defining $Y_n = K_nX_n$, one know that (28) is a sufficient condition by premultiplying and post-multiplying (30) with $\Im$ and using the inequality $-\lceil X_n \circ \tilde{R}_m^{-1}\rceil \le \rho^2\tilde{R}_m - 2\rho X_n$. Similarly, (29) is hold. This completes the proof of Theorem 2. ■

From (9), it is evident that the selection probability β_m^n for each packet varies, resulting in variable controller gains by solving Theorem 2, different from the fixed controller gains in traditional feedback control strategies. Here, Algorithm 1 is presented to clearly illustrate this process. In Algorithm 1, $\bar{\beta}^nm$ denotes the expectation of βm^n, and ε is a given sufficiently small positive constant.

Remark 4: It is noted that frequent updates of β_m^n and K_n will significantly increase computational resource usage. the threshold $\varepsilon \in [0, 1)$ is introduced to reduce the update frequency. Specifically, if the ε is large enough, the VPR-based ETM will be reduced to a case of fixed probability release-based ETM.

TABLE I
PARAMETERS OF THE POWER SYSTEM IN (7) [39]

$\mathscr{P}$	$\mathscr{V}$	$\mathscr{P}$	$\mathscr{V}$	$\mathscr{P}$	$\mathscr{V}$
D	0.0083 (p.u. MW/Hz)	T_t	0.3 (s)	α_g	0.8
R_g	2.4 (Hz/p.u. MW)	M	0.1667 (s)	$\bar{K}_e$	1
ρ_e	0.4167 (p.u. MW/Hz)	T_g	0.08 (s)	α_e	0.2
b	0.425 (p.u. MW/Hz)	T_e	1 (s)		

As discussed in Remark 1, if one sets $l = 1$ for the ETM in (8), it will be degenerated to the TETM. For this situation, the LFC power system can be rewritten as

$$\begin{cases} \dot{x}(t) = Ax(t) + B_u K(e(t) + x(t - \eta(t))) + B_w\omega(t) \\ y(t) = Cx(t). \end{cases} \tag{31}$$

Corollary 1: Given scalars δ and ρ, the system (31) under the TETM in (8) is MSAS with an H_∞ norm bound γ, if there exist symmetric matrices $X > 0$, $\tilde{Q} > 0$, $\tilde{R} > 0$, $\tilde{\Theta} > 0$ and a matrix $\tilde{S}$, such that

$$\begin{bmatrix} \tilde{\Pi}_1 & * \\ \tilde{\Pi}_2 & \tilde{\Pi}_3 \end{bmatrix} < 0 \tag{32}$$

$$\begin{bmatrix} \tilde{R} & * \\ \tilde{S} & \tilde{R} \end{bmatrix} \geq 0 \tag{33}$$

hold, where

$$\begin{aligned} \tilde{\Pi}_1 &= \mathbf{He}\left(\tilde{\mathcal{A}}^T \mathscr{J}_1\right) + \lceil \mathscr{J}_1 \circ \tilde{Q} \rceil + \lceil \mathscr{J}_{l+2} \circ \tilde{Q} \rceil + \lceil \mathcal{C} \circ \tilde{\Gamma} \rceil \\ &\quad + \delta\left(\lceil \left(\mathscr{J}_4 + \mathscr{J}_2\right) \circ \tilde{\Theta} \rceil\right) - \lceil \mathscr{J}_4 \circ \tilde{\Theta} \rceil \\ &\quad - \gamma^2 \lceil \left(\frac{1}{5}\mathbf{1}^T\mathbf{1}\mathscr{J}_\omega\right) \circ I_\omega \rceil \\ \tilde{\Pi}_2 &= \mathbb{C}\{\tau_M \tilde{\mathcal{A}},\ CX\mathscr{J}_1\},\ \tilde{\Pi}_3 = \mathbb{D}\{\rho^2 \tilde{R}_m - 2\rho X,\ -I\} \\ \mathscr{J}_s &= \begin{bmatrix} 0_{5\times 5(s-1)} & I_{5\times 5} & 0_{5\times 5(4-s)} & 0_{5\times 1} \end{bmatrix} \\ \tilde{\mathcal{A}} &= AX\mathscr{J}_1 + B_u Y\mathscr{J}_2 + B_u Y\mathscr{J}_4 + \frac{1}{5}B_\omega \mathbf{1}^T\mathbf{1}\mathscr{J}_\omega \\ \tilde{\mathcal{C}} &= \begin{bmatrix} \mathscr{I}_1^T & \mathscr{I}_2^T & \mathscr{I}_3^T \end{bmatrix}^T \\ \tilde{\Gamma} &= -\lceil \mathcal{Z}_1 \circ \tilde{R} \rceil + \mathbf{He}\left\{\mathcal{Z}_2^T\left(\tilde{R} - \tilde{S}\right)\mathcal{Z}_1\right\} + \mathbf{He}\left\{\mathcal{Z}_3^T \tilde{S} \mathcal{Z}_1\right\} \\ &\quad + \lceil \mathcal{Z}_2 \circ \left(\tilde{S}^T + \tilde{S} - 2\tilde{R}\right) \rceil + \mathbf{He}\left\{\mathcal{Z}_3^T\left(\tilde{R} - \tilde{S}\right)\mathcal{Z}_2\right\} \\ &\quad - \lceil \mathcal{Z}_3 \circ \tilde{R} \rceil. \end{aligned}$$

Furthermore, the controller gain and the weight matrix of the TETM are $K = YX^{-1}$ and $\Theta = \lceil X^{-1} \circ \tilde{\Theta} \rceil$, respectively.

Proof: The proof follows a similar approach to that of Theorem 2, and we omit it here. ■

IV. APPLICATION EXAMPLE

Consider the following LFC power systems with integrated EVs, whose parameters ($\mathscr{P}$) and values ($\mathscr{V}$) are given by Table I.

Assume $\bar{\beta}_1^1 = \bar{\beta}_2^1 = \bar{\beta}_3^1 = 1/3$ and apply Theorem 2 with $\gamma = 10$ and $\rho = 0.5$, we can get the controller gains in the first group

$$K_1 = [-0.0415\ \ -0.1754\ \ -0.5988\ \ -1.1658\ \ -0.4319]$$

$$K_2 = [-0.0438\ \ -0.1776\ -0.6032\ \ -1.1881\ -0.4977]$$

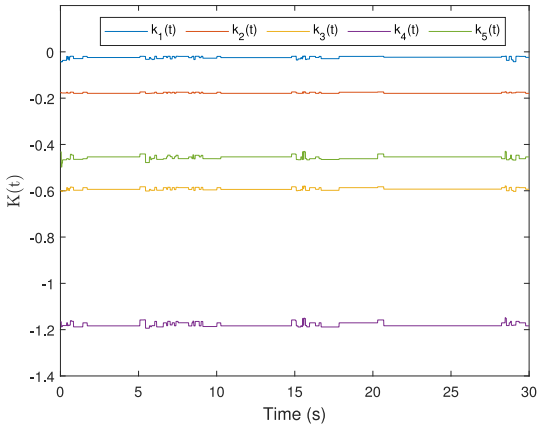

Fig. 3. Variable controller gains $K(t)$ under the proposed VPR-based ETM.

$$K_3 = [-0.0214 - 0.1783\ \ -0.5897\ \ -1.1802\ \ -0.4634]$$

$$\Theta_1 = \begin{bmatrix} 3.2706 & 0.2819 & -2.7698 & 0.1122 & -0.2706 \\ 0.2819 & 6.7558 & 1.0174 & -3.2968 & 0.4086 \\ -2.7698 & 1.0174 & 4.2072 & -2.2978 & 0.4577 \\ 0.1122 & -3.2968 & -2.2978 & 3.3794 & -0.3983 \\ -0.2706 & 0.4086 & 0.4577 & -0.3983 & 0.1018 \end{bmatrix}$$

$$\Theta_2 = \begin{bmatrix} 3.1174 & 0.1028 & -2.6766 & 0.2057 & -0.2790 \\ 0.1028 & 5.9269 & 0.9355 & -2.8498 & 0.4283 \\ -2.6766 & 0.9355 & 3.7669 & -1.9823 & 0.4665 \\ 0.2057 & -2.8498 & -1.9823 & 2.8746 & -0.4100 \\ -0.2790 & 0.4283 & 0.4665 & -0.4100 & 0.1012 \end{bmatrix}$$

$$\Theta_3 = \begin{bmatrix} 3.0519 & -0.1925 & -2.6036 & 0.3382 & -0.3134 \\ -0.1925 & 5.2336 & 0.8618 & -2.3537 & 0.4213 \\ -2.6036 & 0.8618 & 3.3553 & -1.7286 & 0.4763 \\ 0.3382 & -2.3537 & -1.7286 & 2.4288 & -0.4074 \\ -0.3134 & 0.4213 & 0.4763 & -0.4074 & 0.1093. \end{bmatrix}$$

Assume the initial state $x(0) = [1\ \ 0\ \ 0.2\ \ 0\ \ 3]^T$ and the disturbance, as given in [39], is by

$$\omega(t) = \begin{cases} 0.01\sin(t), & \text{if } t \in [0,\ 20] \\ 0, & \text{if } t \in (20,\ \infty). \end{cases}$$

According to Algorithm 1, with $\delta = 0.1$ and $\varepsilon = 10^{-6}$, the controller gains, denoted by $K_n(t)$ within the nth group, can be determined. These gains are depicted in Fig. 3. It is observed that the controller gains vary within each group sequence, demonstrating their ability to adapt to state variations under the VPR-based ETM.

By applying the control strategy in (16) alongside the VPR-based ETM in (8), we can analyze the state responses of the LFC power systems as well as the release instants and intervals (RIIs), as depicted in Figs. 4 and 5, respectively. Observing Fig. 4, it is clear that the settling time is approximately 10 s. In contrast, using the method outlined in [8] results in a settling time of around 18 s. This demonstrates that our approach offers superior control performance for LFC power systems. Fig. 5 reveals that numerous redundant packets are discarded, thereby reducing the network burden. Simultaneously, the 'necessary' data with significant variations are transmitted over the network. To maintain good system stability performance, variable control gains are imperative to adapt to these state

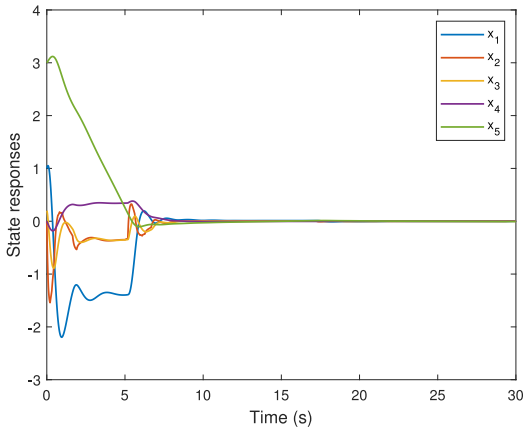

Fig. 4. State responses of the system (17) under the VPR-based ETM.

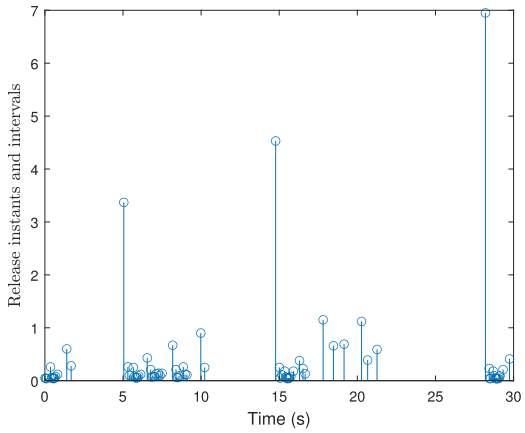

Fig. 5. RIIs of the system (17) under the VPR-based ETM.

fluctuations. By combining insights from Figs. 3 and 5, it becomes apparent that the control gains change more significantly during periods with a higher frequency of triggering events, such as the intervals between 5–10 and 15–18 s.

To validate the advantages of the proposed VPR-based ETM for the LFC power systems, we consider the following two cases, both applied to the same LFC power systems as above, in what follows.

Case 1 (LFC Power Systems Under the TETM): Applying Corollary 1 with $\gamma = 10$ and $\rho = 0.5$, one can get the controller gain K and the weight matrix of the TETM as follows:

$$K = [-0.0145 \ -0.0909 \ -0.2860 \ -0.5747 \ -0.2732]$$

$$\Theta = \begin{bmatrix} 6.7249 & 0.8749 & -7.2933 & 2.6550 & -1.1065 \\ 0.8749 & 73.7920 & -13.0780 & -5.5884 & 1.7311 \\ -7.2933 & -13.0780 & 10.7860 & -3.1935 & 1.1604 \\ 2.6550 & -5.5884 & -3.1935 & 3.5859 & -1.0279 \\ -1.1065 & 1.7311 & 1.1604 & -1.0279 & 0.3414 \end{bmatrix}.$$

Figs. 6(a) and 7(a) depict the state responses and RIIs of the LFC power system (31), respectively. Table II shows the number of ARPs, denoted as $\mathscr{T}$, and DRRs, denoted as $\mathscr{D}$. Comparing Fig. 4 with Fig. 6(a) and observing Table II, it is evident that our proposed VPR-based ETM achieves superior control performance compared to adopting the TETM,

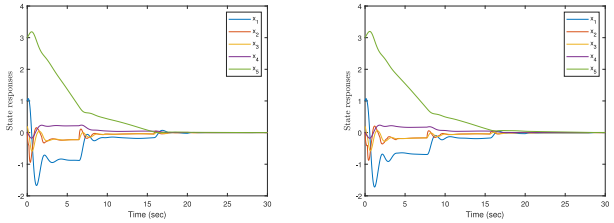

Fig. 6. State responses of the system (31). (a) Under case 1. (b) Under case 2.

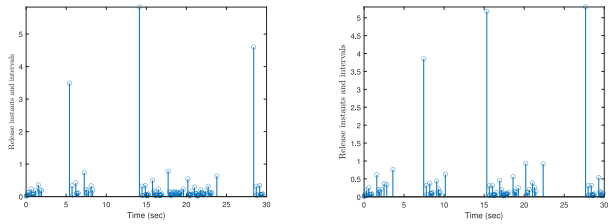

Fig. 7. RIIs of the system (31). (a) Under case 1. (b) Under case 2.

while consuming less network bandwidth. This enhanced performance is primarily attributed to dynamic adjustment of controller gains and more effective selection of 'essential' packets.

To further validate the effectiveness and superiority of the mechanism designed in this article, we next adopt the DETM proposed in [15] for comparison.

Case 2 (LFC Power Systems Under the DETM): As in [15], the dynamic threshold is designed by

$$\delta(t) = \delta - \delta \tanh(f(t)), t \in [t_k h + \eta_k, t_{k+1} h + \eta_{k+1}) \quad (34)$$

where $f(t) = (l(t) - l(t_k))/l(t)$, $l(t) = t_k h + jh$ and $l(t_k) = t_k h$ denote the current sampling instant and the previous triggered instant, respectively.

The DETM with threshold (34) can be designed as

$$t_{k+1} h = t_k h + \min_{j \in N} \{jh | \Psi(e(t), x(t_k h), \delta(t)) > 0\} \quad (35)$$

where the definitions of the variables are similar to those in (8), except for the triggering threshold defined in (34).

Under the same conditions as case 1, the state responses of the LFC power system (31) using the DETM (35) are shown in Fig. 6(b). The RIIs are depicted in Fig. 7(b), and the time-varying threshold is shown in Fig. 8. Comparing Fig. 4 with 6(b), one can see that the LFC power system using our proposed VPR-based ETM exhibits faster state responses. Moreover, the comparison of DRRs in Table II shows that our method can further reduce network resource consumption. These improvements are mainly attributed to the enhanced packet discarding mechanism based on the TETM and the adaptation of time-varying controller gains.

V. Conclusion

In this article, a novel VPR-based ETM and intermittently updated controller gains have been developed for LFC power

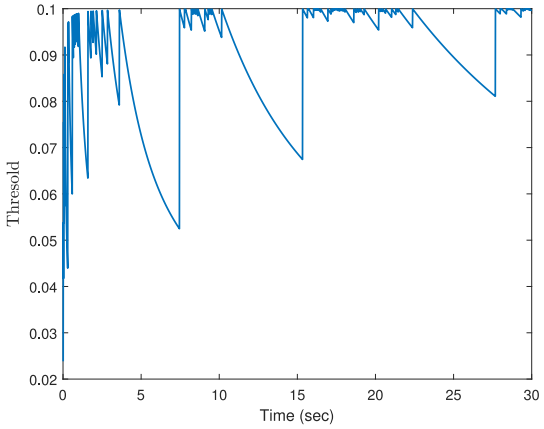

Fig. 8. Threshold of the DETM.

TABLE II
$\mathscr{T}$ AND $\mathscr{D}$ OF THE LFC POWER SYSTEM WITHIN [0, 30] S

Communication mechanisms	$\mathscr{T}$	$\mathscr{D}$
TETM in [37]	124	4.13%
DETM in [15]	96	3.20%
Our proposed VPR-based ETM	80	2.67%

systems integrated with EVs. Based on the TETM, a VPR scheme is designed to pick a triggered packet from each group for transmission. The ARP is selected according to the transmission probability updated in response to system states. A buffer, integrated after the TETM, ensures the ARP is transmitted at the last triggered instant of each group sequence, thereby conserving network bandwidth. Moreover, the designed controller gains are updated at each group sequence, resulting in better-control performance. While this approach consumes more computational resources, the reduced number of triggering events may compensate for this flaw. Future research will focus on: 1) refining the ETM by incorporating ideas from DETM and memory-based ETMs, and improving the update mechanism for transmission probabilities and 2) considering more complex scenarios for power systems, such as multiarea power systems, and the power systems integrated with capacity-limited EVs.

REFERENCES

[1] V. Çelik, M. T. Özdemir, and K. Y. Lee, "Effects of fractional-order PI controller on delay margin in single-area delayed load frequency control systems," *J. Mod. Power Syst. Clean Energy*, vol. 7, pp. 380–389, Mar. 2019.

[2] S. Kuppusamy and Y. H. Joo, "Resilient reliable H_θ load frequency control of power system with random gain fluctuations," *IEEE Trans. Syst. Man Cybern. Syst.*, vol. 52, no. 4, pp. 2324–2332, Apr. 2022.

[3] H. Shen, D. Wang, J. H. Park, V. Sreeram, and J. Wang, "Switching-like event-triggered sliding mode load frequency control for networked power systems under energy-limited DoS attacks," *IEEE Trans. Syst. Man Cybern. Syst.*, vol. 54, no. 3, pp. 1589–1598, Mar. 2024.

[4] X. Li and D. Ye, "Event-based distributed fuzzy load frequency control for multiarea nonlinear power systems with switching topology," *IEEE Trans. Fuzzy Syst.*, vol. 30, no. 10, pp. 4262–4272, Oct. 2022.

[5] M. Khan and H. Sun, "Complete provision of MPC-based LFC by electric vehicles with inertial and droop support from DFIG-based wind farm," *IEEE Trans. Power Del.*, vol. 37, no. 2, pp. 716–726, Apr. 2022.

[6] T. N. Pham, A. M. T. Oo, and H. Trinh, "Event-triggered mechanism for multiple frequency services of electric vehicles in smart grids," *IEEE Trans. Power Syst.*, vol. 37, no. 2, pp. 967–981, Mar. 2022.

[7] F. Babaei, Z. B. Lashkari, A. Safari, M. Farrokhifar, and J. Salehi, "Salp swarm algorithm-based fractional-order PID controller for LFC systems in the presence of delayed EV aggregators," *IET Electr. Syst. Transp.*, vol. 10, no. 3, pp. 259–267, Sep. 2020.

[8] G. Liu, J. H. Park, C. Hua, and Y. Li, "Hybrid dynamic event-triggered load frequency control for power systems with unreliable transmission networks," *IEEE Trans. Cybern.*, vol. 53, no. 2, pp. 806–817, Feb. 2023.

[9] B. Li and J. Wu, "Adaptive assessment of power system transient stability based on active transfer learning with deep belief network," *IEEE Trans. Autom. Sci. Eng.*, vol. 20, no. 2, pp. 1047–1058, Apr. 2023.

[10] A. Sari, Ç. Sönmez, S. Ayasun, and Y. Kabalci, "Delay-dependent stability analysis of multi-area LFC-EVs system," *IEEE Trans. Smart Grid*, vol. 14, no. 3, pp. 2178–2188, May 2023.

[11] S. Tripathi, V. P. Singh, N. Kishor, and A. S. Pandey, "Load frequency control of power system considering electric Vehicles' aggregator with communication delay," *Int. J. Electr. Power Energy Syst.*, vol. 145, Feb. 2023, Art. no. 108697.

[12] X. Liu et al., "Event-triggering load frequency control for multi-area power system based on random dynamic triggering mechanism and two-side closed functional," *ISA Trans.*, vol. 133, pp. 193–204, Feb. 2023.

[13] Y. Wang, Z. Wang, J. Gan, H. Zhang, and R. Wang, "Switched observer-based adaptive event-triggered load frequency control for networked power systems under aperiodic DoS attacks," *IEEE Trans. Smart Grid*, vol. 14, no. 6, pp. 4816–4826, Nov. 2023.

[14] J. Liu, Y. Gu, L. Zha, Y. Liu, and J. Cao, "Event-triggered H_∞ load frequency control for multiarea power systems under hybrid cyber attacks," *IEEE Trans. Syst. Man Cybern. Syst.*, vol. 49, no. 8, pp. 1665–1678, Aug. 2019.

[15] P. Chen, D. Zhang, L. Yu, and H. Yan, "Dynamic event-triggered output feedback control for load frequency control in power systems with multiple cyber attacks," *IEEE Trans. Syst. Man Cybern. Syst.*, vol. 52, no. 10, pp. 6246–6258, Oct. 2022.

[16] X.-C. Shangguan et al., "Robust load frequency control for power system considering transmission delay and sampling period," *IEEE Trans. Ind. Informat.*, vol. 17, no. 8, pp. 5292–5303, Aug. 2021.

[17] Z. Huo and B. Wang, "Distributed resilient multi-event cooperative triggered mechanism based discrete sliding-mode control for wind-integrated power systems under denial of service attacks," *Appl. Energy*, vol. 333, Mar. 2023, Art. no. 120636.

[18] C. Li, X. Zhao, M. Chen, W. Xing, N. Zhao, and G. Zong, "Dynamic periodic event-triggered control for networked control systems under packet dropouts," *IEEE Trans. Autom. Sci. Eng.*, vol. 21, no. 1, pp. 906–920, Jan. 2024.

[19] Y. Gu, Z. Sun, L.-W. Li, J. H. Park, and M. Shen, "Event-triggered security adaptive control of uncertain multi-area power systems with cyber attacks," *Appl. Math. Comput.*, vol. 432, Nov. 2022, Art. no. 127344.

[20] Z. Gu, P. Shi, D. Yue, S. Yan, and X. Xie, "Memory-based continuous event-triggered control for networked T–S fuzzy systems against cyberattacks," *IIEEE Trans. Fuzzy Syst.*, vol. 29, no. 10, pp. 3118–3129, Oct. 2021.

[21] L. Yao and X. Huang, "Memory-based adaptive event-triggered secure control of Markovian jumping neural networks suffering from deception attacks," *Sci. China Technol. Sci.*, vol. 66, pp. 468–480, Feb. 2023.

[22] J. Song, D. Shi, H. Yu, Y. Shi, and J. Wang, "A dynamic proportional-integral based event-triggered output feedback control framework for networked mechatronic system," *IEEE Trans. Ind. Electron.*, vol. 70, no. 8, pp. 8344–8354, Aug. 2023.

[23] C. Du, F. Li, Y. Shi, C. Yang, and W. Gui, "Integral event-triggered attack-resilient control of aircraft-on-ground synergistic turning system with uncertain tire cornering stiffness," *IEEE/CAA J. Automatica Sinica*, vol. 10, no. 5, pp. 1276–1287, May 2023.

[24] L. Xie, J. Cheng, Y. Zou, Z.-G. Wu, and H. Yan, "A dynamic-memory event-triggered protocol to multiarea power systems with semi-Markov jumping parameter," *IEEE Trans. Cybern.*, vol. 53, no. 10, pp. 6577–6587, Oct. 2023.

[25] D. Ding, Z. Tang, J. H. Park, and Z. Ji, "Quasi-bipartite synchronization of derivatively coupled complex dynamic networks: Memory-based self-triggered approach," *IEEE Trans. Syst. Man Cybern. Syst.*, vol. 54, no. 3, pp. 1611–1621, Mar. 2024.

[26] Z. Gu, D. Yue, C. K. Ahn, S. Yan, and X. Xie, "Segment-weighted information-based event-triggered mechanism for networked control systems," *IEEE Trans. Cybern.*, vol. 53, no. 8, pp. 5336–5345, Aug. 2023.

[27] X.-G. Guo, D.-Y. Zhang, J.-L. Wang, J. H. Park, and L. Guo, "Observer-based event-triggered composite anti-disturbance control for multi-agent systems under multiple disturbances and stochastic FDIAs," *IEEE Trans. Autom. Sci. Eng.*, vol. 20, no. 1, pp. 528–540, Jan. 2023.

[28] Z. Hu and X. Mu, "Event-triggered impulsive control for stochastic networked control systems under cyber attacks," *IEEE Trans. Syst. Man Cybern. Syst.*, vol. 52, no. 9, pp. 5636–5645, Sep. 2022.

[29] Q. Hou and J. Dong, "Distributed dynamic event-triggered consensus control for multiagent systems with guaranteed L_2 performance and positive inter-event times," *IEEE Trans. Autom. Sci. Eng.*, vol. 21, no. 1, pp. 746–757, Jan. 2024.

[30] S. Han, H. Zhu, Q. Zhong, K. Shi, and O.-M. Kwon, "Adaptive event-triggered fuzzy positioning control for unmanned marine vehicles with actuator saturation and hybrid attacks," *IEEE Trans. Fuzzy Syst.*, vol. 31, no. 9, pp. 3055–3068, Sep. 2023.

[31] X. Wang, D. Ding, X. Ge, and H. Dong, "Neural-network-based control with dynamic event-triggered mechanisms under DoS attacks and applications in load frequency control," *IEEE Trans. Circuits Syst. I, Reg. Papers*, vol. 69, no. 12, pp. 5312–5324, Dec. 2022.

[32] Y. Liu, Y. Chen, and M. Li, "Dynamic event-based model predictive load frequency control for power systems under cyber attacks," *IEEE Trans. Smart Grid*, vol. 12, no. 1, pp. 715–725, Jan. 2021.

[33] J. Wang, D. Wang, L. Su, J. H. Park, and H. Shen, "Dynamic event-triggered H_∞ load frequency control for multi-area power systems subject to hybrid cyber attacks," *IEEE Trans. Syst., Man, Cybern., Syst.*, vol. 52, no. 12, pp. 7787–7798, Dec. 2022.

[34] J. Yang, Q. Zhong, K. Shi, and S. Zhong, "Dynamic-memory event-triggered H_∞ load frequency control for reconstructed switched model of power systems under hybrid attacks," *IEEE Trans. Cybern.*, vol. 53, no. 6, pp. 3913–3925, Jun. 2023.

[35] H. Yu and T. Chen, "Periodic event-triggered networked control systems subject to large transmission delays," *IEEE Trans. Autom. Control*, vol. 68, no. 1, pp. 63–79, Jan. 2023.

[36] T. N. Pham, S. Nahavandi, L. V. Hien, H. Trinh, and K. P. Wong, "Static output feedback frequency stabilization of time-delay power systems with coordinated electric vehicles state of charge control," *IEEE Trans. Autom. Control*, vol. 32, no. 5, pp. 3862–3874, Sep. 2017.

[37] D. Yue, E. Tian, and Q.-L. Han, "A delay system method for designing event-triggered controllers of networked control systems," *IEEE Trans. Autom. Control*, vol. 58, no. 2, pp. 475–481, Feb. 2013.

[38] D. Liu and D. Ye, "Secure synchronization against link attacks in complex networks with event-triggered coupling," *Inf. Sci.*, vol. 628, pp. 291–306, May 2023.

[39] E. Tian and C. Peng, "Memory-based event-triggering H_∞ load frequency control for power systems under deception attacks," *IEEE Trans. Cybern.*, vol. 50, no. 11, pp. 4610–4618, Nov. 2020.